ADVANCED MATERIALS
www.advmat.de

Solvent-Assisted 4D Programming and Reprogramming of Liquid Crystalline Organogels

*Binjie Jin, Jiaqi Liu, Yunpeng Shi, Guancong Chen, Qian Zhao, and Shu Yang**

Encoding molecular ordering during liquid crystalline network (LCN) formation endows preprogrammed but fixed shape morphing in response to external stimuli. The incorporation of dynamic covalent bonds enables shape reprogramming but also permanently alters the network structures. Here, an entropic approach that can program complex shapes via directed solvent evaporation from an isotropic LCN organogel is discoursed. Different shapes can be erased and reprogrammed from the same LCN on demand depending on the modes of deformation of the organogel during solvent evaporation. The ability to decouple network synthesis and molecular alignment relaxes the requirements to LCN chemistry and alignment methods, allowing for the realization of a variety of origami/kirigami structures and 4D shape morphing of LCNs printed from the digital light processing technique with unattainable spatial and temporal controls.

1. Introduction

Liquid crystal elastomers (LCEs), known for their geometric, mechanical, magnetic, optical, and electronic anisotropy and soft elasticity, are of great interests for stimuli-responsive shape morphing, sensing, actuations, and displays.[1] To direct the shape change, preprogramming liquid crystal (LC) molecular ordering during the network formation is essential. Strategies such as applications of mechanical force and a magnetic or electric field, guided surface alignment, and shear extrusion are commonly used, followed by crosslinking to lock the mesogenic ordering within the network.[2] The transformed shape is deterministic due to the covalent nature of the network. To generate a new shape, a new film needs to be fabricated. Functional nanofillers have been introduced in LCEs to transduce heat, allowing for shape reprogramming.[3,4] Nevertheless, nanofillers significantly increase the viscosity of the precursors, making alignment challenging, thus reducing the achievable strains.

LCEs with dynamic covalent bonds have been studied for shape reprogramming,[5] where the network connectivity can be permanently altered and form a new mesogenic distribution, which, however, could also disrupt the LC phase within the network. So far, most LCE/dynamic bond systems are based on heat-induced bond change and the shape change is achieved by remolding or welding films together of relatively simple geometries, such as thin strips, where the anisotropic alignment of LC molecules are induced by mechanical stretching or creep in the bulk polymer films. Furthermore, the network rearrangement induced by dynamic covalent bonds essentially is a cumulative plastic flow, that is, once reconfigured, the networks are never the same as the original one. Therefore, it will be highly desirable to devise a simple yet versatile strategy that can reprogram LC ordering at the microscale without altering the chemical nature of the network, yet providing spatial and temporal control in three dimensions to achieve more complex geometries.

Additive manufacturing offers new opportunities to create 4D LCEs.[6] Among different techniques, direct ink writing (DIW) is the most widely used since the LC mesogens can be readily aligned during ink extrusion.[6a,b,c] Nonetheless, it is critical to fine control the printing parameters to achieve nozzle-based shear thinning of LCE precursors. Use of an external field, such as the magnetic field, has also been explored to encode mesogenic alignment.[6d,e] However, the setup and control of the magnetic field are much more complex compared with shearing thinning or mechanical deformation, especially in 3D space. In layer-by-layer printing, a long dwell time (5 min per alignment) is needed between layers.[6e] Multiphoton polymerization of LCEs has also been attempted,[6f] where each layer is sandwiched between two rubbered sacrificial during printing. Therefore, the approach is cumbersome and time-consuming.

Herein, we report an entropic approach to program and reprogram shapes intrinsically from a wide range of neat LC organogels infused with solvent in the form of 2D sheets or 3D constructs printed from the digit light processing (DLP) technique. Solvent, often considered detrimental to mesogenic alignment in LC networks (LCNs) and should be removed before programming, here plays a central role to assist the programming and reprogramming of the 4D shape morphing. We align the mesogens in the fully crosslinked LCN via solvent evaporation of the organogel under stress, which physically locks the programmed LC director fields, and the alignment can be erased by reswelling LCN in a solvent. This solvent-assisted programming is orthogonal to the temperature-activated

B. Jin, J. Liu, S. Yang
Department of Materials Science and Engineering
University of Pennsylvania
3231 Walnut Street, Philadelphia, PA 19104, USA
E-mail: shuyang@seas.upenn.edu
B. Jin, Y. Shi, G. Chen, Q. Zhao
Department of Chemical Engineering and Biological Engineering
Zhejiang University
38th Zheda Road, Zhejiang 310027, China
The ORCID identification number(s) for the author(s) of this article can be found under https://doi.org/10.1002/adma.202107855.

DOI: 10.1002/adma.202107855

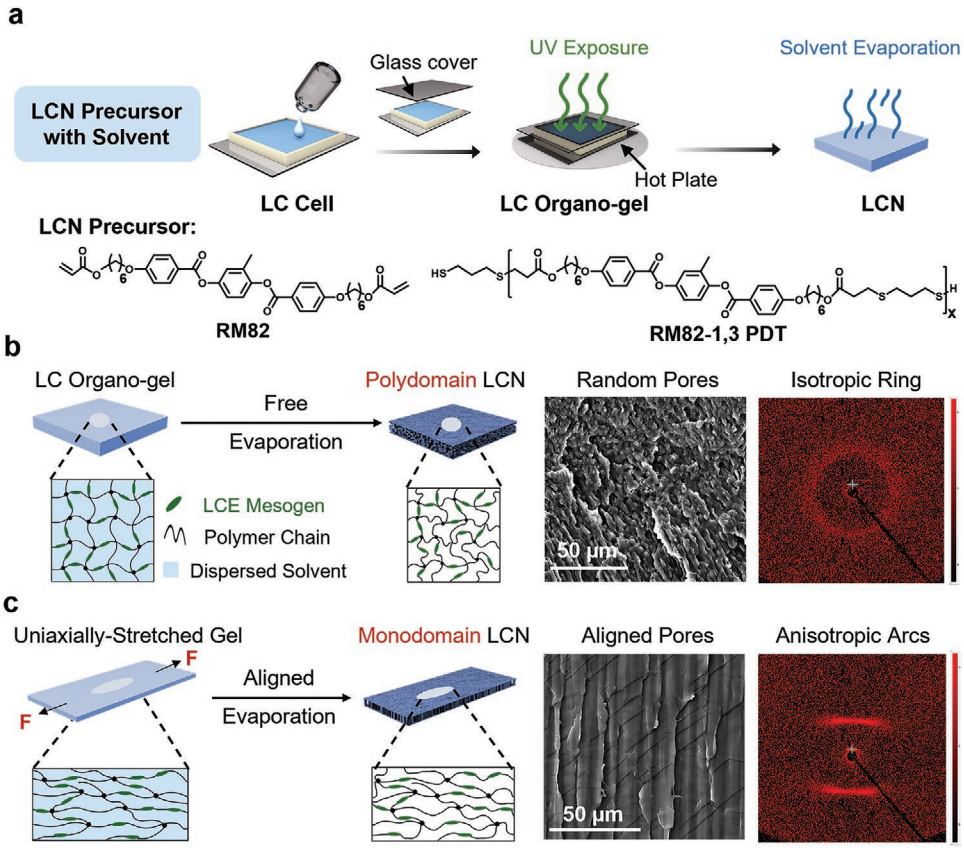

Figure 1. a) Synthesis of the LC organogel and formation of LCN via solvent evaporation. b) Schematic illustrations of the formation of polydomain LCN via free solvent evaporation. Inset: Cross-sectional SEM images and 2D WAXD images. c) Schematic illustrations of the formation of monodomain LCN via aligned solvent evaporation (uniaxial stretching). Inset: Cross-sectional SEM images and 2D WAXD images.

LC phase transition, enabling the LCNs to be stably actuated between the temporary and permanent shapes. Since there is no plastic deformation of the network, the temporary shapes can always return to their original state on demand. The ability to decouple network synthesis from the mesogen alignment offers unparallel dexterity to program 4D shapes from free-form DLP printing and origami or kirigami folding strategies from a wide range of LCN chemistry. We note while the shape morphing reported here is from LCEs, we refer to our system as LCNs since the solvent-assisted programming approach is not limited to LCEs.

2. Results and Discussion

First, we create an isotropic organogel by crosslinking the precursors from established thiol–ene click chemistry[7] in a miscible organic solvent. The LC oligomers (LCO, $\overline{M_w}$ = 2708; see characterization in Figure S1a in the Supporting Information), RM82-1,3 PDT, synthesized from a reactive mesogenic monomer, 1,4-bis-[4-(6-acryloyloxy-hexyloxy)benzoyloxy]-2-methylbenzene (RM82) with a chain extender, 1,3-propanedithiol (1,3-PDT; see details in the Experimental Section), and RM82 are each dissolved in a good solvent, including dimethyl chloride (DCM), toluene, or *N*,*N*-dimethylformamide (DMF), before mixing in 1:1 molar ratio for UV curing as shown in **Figure 1**a. The choice of a good solvent is important to ensure the network is swollen extensively such that voids could be generated as the polymer chains collapse during drying. Thus, the initial conformation of the gel state shall play a critical role in alignment programing. Since solvent swelling is isotropic itself, when the solvent is freely evaporated as a control reference, polydomains are formed (Figure 1b), which is confirmed by the 2D wide-angle X-ray diffraction (WAXD) pattern, showing a uniform ring in Figure 1b. Meanwhile, the molecular rigidity of LC mesogens will hinder chain relaxation during the solvent-loss-induced volume shrinkage,[8] leading to the formation of micropores in the dry film, as manifested by scanning electron microscopy (SEM) images (Figure 1b; Figure S2, Supporting Information). In comparison, the neat LCN film prepared from the LC precursor without solvent shows no pores (Figure S3, Supporting Information). The freely evaporated sample shows randomly distributed micropores. To create a uniform alignment of LC mesogens (i.e., monodomains), we uniaxially stretch the swollen network, followed by evaporation in the deformed state. As seen from the 2D WAXD pattern, two distinct arcs are observed (Figure 1c) and their relative positions suggest the nematic directors are along the stretching direction (0° and 180°), which is confirmed by polarized optical microscopy (POM) images (Figure S4, Supporting Information). The cross-sectional SEM image shows that pores are well-aligned along the film thickness direction, perpendicular to the in-plane mechanical stretching direction

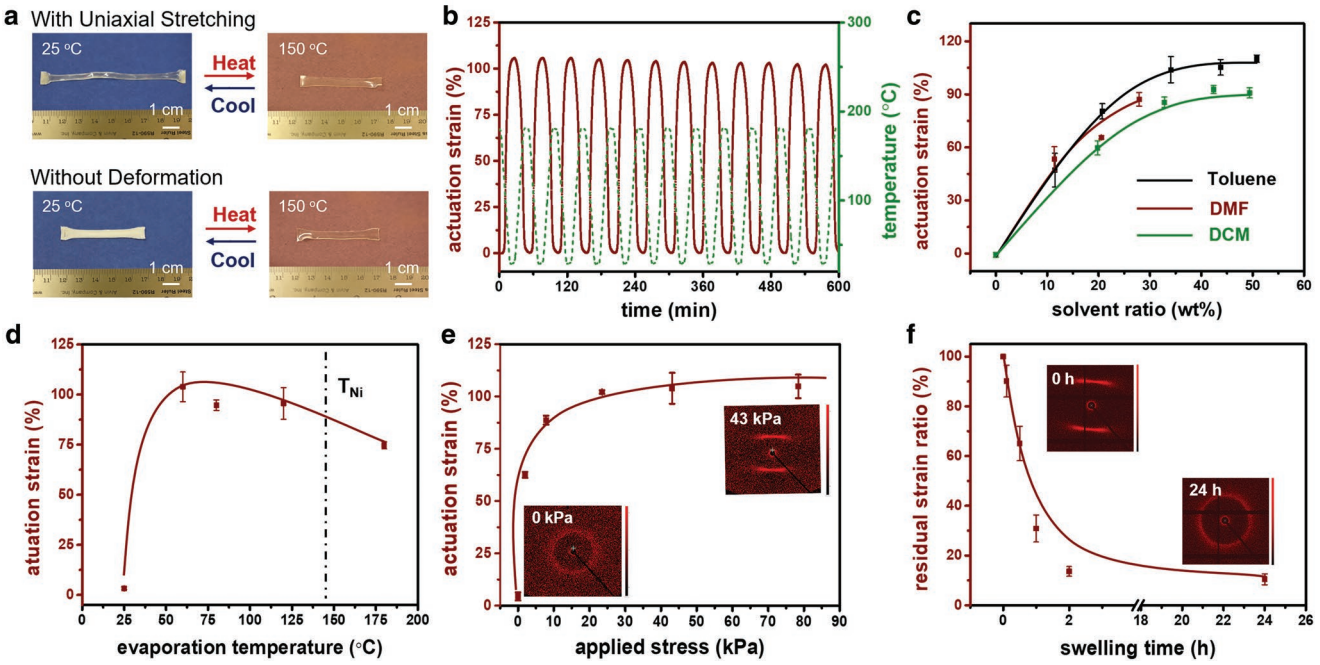

Figure 2. a) Photos of the actuation behaviors from samples with solvent evaporated under uniaxial stretching (applied stress = 43 kPa) and without deformation, respectively (T_{eva} = 60 °C, 35 wt% toluene). b) DMA cyclic actuation curves of the uniaxially stretched sample shown in panel (a). c) The actuation strain as a function of the solvent (applied stress = 43 kPa, T_{eva} = 60 °C). d) The actuation of strain as a function of evaporation temperature, T_{eva} (applied stress = 43 kPa, 35 wt% toluene). e) The dependence of actuation strain on the applied force during solvent evaporation (T_{eva} = 60 °C, 35 wt% toluene). Inset: 2D WAXD images from samples evaporated under a constant stress, 0 and 43 kPa, respectively. f) The relationship between the normalized residual strain and the toluene swelling time. Inset: 2D WAXD images from samples swelled by toluene for 0 and 24 h, respectively.

due to conservation of the volume (see Figure 1c and Figure S2 in the Supporting Information).

To validate the entropically driven programmability of the LCN, we characterize the film's actuation performance. As shown in **Figure 2**a, the uniaxially stretch-evaporated LCE film (applied stress, 43 kPa) shows ≈100% reversible length change (the correlation between strain and temperature can be founded Figure S5 in the Supporting Information), whereas the freely evaporated one was inactive (Videos S1 and S2, Supporting Information) upon heating above the nematic-to-isotropic transition temperature (T_{NI}), ≈140 °C, which was measured from differential scanning calorimetry (DSC) (Figure S6, Supporting Information). This temperature is similar to that of conventionally prepared LCE from RM82-1,3 PDT,[7] although the strain doubles due to the prestretching. Indeed, little actuation is observed in LCNs synthesized from the neat mixture (RM82 and LCO) after thermal annealing (whether uniaxially stretched or not; see Figure S7 in the Supporting Information), confirming the necessity of solvent in our approach. The stability of the actuation is further confirmed by dynamic mechanical analysis (DMA) (Figure 2b). The nearly identical strain-temperature curves in repeated cooling–heating cycles suggest that the physically fixed mesogenic alignment is not disturbed by the temporal chain segmental (or mesogenic) movements during the LC phase change. Further we show that the LCN actuation is highly resilient (Figure S8, Supporting Information). Here, the resilience is defined as: $\phi(\%) = \frac{\lambda_x}{\lambda_1} \times 100\%$, where λ_x is the actuation strain in cycles x and λ_1 is the actuation strain in the first cycle, respectively.

Conventionally, the preprogrammed mesogenic alignment is fixed via chemical crosslinking of the network.[2a] Naturally, we ask what may act as the "crosslinking sites" in our approach to memorize the aligned state of the LC mesogens upon drying under deformation since there is no chemical reaction in the whole process. When LCN synthesized from the neat mixture (RM82 and LCO) was uniaxially stretched, followed by thermal-annealing overnight (to mimic the solvent evaporation assisted programming), no micropores nor reversible actuation was observed (see Figures S3 and S7 in the Supporting Information). Therefore, micropores formed during drying must act as the physical "crosslinking sites" to memorize the programmed LC director field. It is worth mentioning that similar microporous structures have been reported in hydrogels and isotropic organogels after drying.[9,10] However, these pores collapse permanently after heating above their crystallization or glass transition temperature. Therefore, the highly reversible memory effect of our system (see Figure 2b and Figure S8 in the Supporting Information) suggests that the pores must be recovered upon cooling. When the temperature is heated above T_{NI}, LC mesogens will undergo fast nematic-to-isotropic transition. The chain movement and the corresponding shrinkage of the film in the aligned direction lead to collapsed pores that store the elastic energy. If the stored elastic energy is released due to chain relaxation,[9,10] pores will be permanently closed, thus the actuation cannot be fully recovered. Since the chain mobility of LCNs is restricted by the rigid mesogens, chain relaxation does not occur during the cyclic heating and cooling (about 50 min per cycle in Figure 2d, which is determined by the ramping rate

of the temperature). Upon cooling below T_{NI}, the stored elastic energy is released to restore the temporarily collapsed pores.

The efficiency of alignment programming can be estimated by the actuation strain, defined as $100\% \times (L_{cold} - L_{hot})/L_{hot}$, where L_{cold} and L_{hot} are the sample lengths at 25 and 150 °C, respectively. Since the LC director field is stabilized via the micropores, the porosity can be analogous to the "degree of crosslinking," determined by the solvent mass ratio percentage. As seen in Figure 2c, for samples of the same dimensions (50 mm × 12.5 mm × 0.4 mm) and undergone the same evaporation temperature and applied stress, the actuation strain increases with the solvent mass ratio percentage and eventually reaches a plateau. The solvent evaporation rate is critically important to the kinetics of micropore formation. Here, we investigate three good solvents, including DCM, toluene, and DMF with descending evaporation rates. They are completely evaporated at 60 °C overnight, confirmed by the thermogravimetric analysis (TGA; Figure S9, Supporting Information). Samples from toluene, which has an intermediate evaporation rate, endows the largest actuation strain, whereas samples dried from DCM, which has the highest evaporation rate, show the lowest actuation strain. These suggest that the rate of solvent evaporation should match with the chain reconfiguration rate; as the solvent evaporates, the chain mobility is also suppressed. Supporting this, LCN from DMF, which has the lowest evaporation rate, and thus the chains have the longest time for relaxation, shows intermediate actuation strain among the three with the smallest porosity (Figure S10, Supporting Information). Accordingly, LC gel with 35 wt% toluene is selected for the studies discussed next.

We now investigate evaporation temperature (T_{eva}) and applied stress to the actuation strain. As shown in Figure 2d, actuation strain initially ascends with the increasing T_{eva} until reaching a plateau but decreases once above T_{NI}. This is because as temperature increases, chain mobility also increases, promoting the network reconfiguration to program the LC director field. Above T_{NI}, the stretched network begins to recover, thus decreasing in actuation strain. Thus, 60 °C is chosen as the T_{eva}. Since the fixed LC director field is programmed by the mechanical deformation along with solvent evaporation, the actuation strain is expected to be dependent on the applied stress. Indeed, Figure 2e confirms that the actuation strain increases with the applied stress, reaching saturation (≈105%) at an applied stress of ≈40 kPa. We believe this saturation arises from the increased modulus as the solvent evaporates, with no further deformation after 1 h evaporation. Therefore, the maximum strains under different initial applied stresses are nearly identical (Figure S11, Supporting Information). We note that LC organogels are more prone to break at a higher applied stress. At another front, only the mesogenic alignment induced by the elastic deformation can be effectively memorized according to the programming mechanism, which is determined by the integrity of the network. Therefore, as shown in Figure S12 in the Supporting Information, the actuation can be tuned by the UV curing time.

Since LCN synthesis and mesogenic alignment can be completely decoupled in our approach, we no longer need to concern whether crosslinking or bond exchange in the network would interfere with LC ordering for reprogramming as reported in the literature.[2a,5] As shown in Table S1 and Figure S13 in the Supporting Information, the entropic alignment principle could be applied to a wide variety of LC monomers and chain extenders, achieving actuation strains from 39% to 109%. Although mechanical prestretching has been applied to a partially polymerized LC film[2a] and 3D printed structures,[11] the resulting LCNs cannot be reprogrammed once crosslinked. In contrast, we fully take advantage of the solvent such that the preprogrammed shape in our LCNs can be erased by reswelling the film in toluene, followed by free evaporation. As seen from WAXD patterns (Figure 2f), the two distinct arcs merge into an isotropic ring, suggesting the LC alignment is erased. Cross-sectional SEM images confirm that the porous structures change from vertically aligned ones to randomly distributed (Figure S14, Supporting Information). Correspondingly, this elastic reprogramming of network conformation drives the film to recover to its original (or permanent) shape, in contrast to LCNs with dynamic covalent bonds, where plastic deformation occurs. By virtual, the LCN can be reprogrammed into infinite temporary shapes by programming the solvent evaporation modes. We noted that the residual strain should be swelling time-independent and decrease to zero after the network is fully relaxed. Nonetheless, we find that the residual strain is still registered in the sample even after 24 h, which can be attributed to the fact that a complete network relaxation is not easy to achieve due to the somewhat restricted chain mobility in a crosslinked network. Longer swelling time or heating during swelling could accelerate the relaxation processing. However, it will also weaken the network's mechanical strength, reducing its ability for repeated programming and reprogramming. In our experiments, despite not achieving zero strain after swelling over 24 h, LCN undergoes repeated actuation cycles if we maintain the same heating/cooling cycles.

The ability to encode molecular alignment in an initially homogenous gel via spatial deformation along with solvent evaporation will allow us to generate a wide variety of nonlinear actuation responses from a single film. As depicted in **Figure 3**a, the initial rectangular LC organogel could be readily programmed into three different 3D structures, demonstrating reversible actuation behaviors, including bending, waving, and twisting at will. Below T_{NI}, the shape is determined by the directed solvent evaporation, which can be erased and reprogrammed, which we refer as the temporary shape. Above T_{NI} (e.g., 150 °C), the transformed shape is defined by the mold during the network synthesis, which we refer as the permanent shape. As illustrated in Figure 3b and Video S3 in the Supporting Information, the nonlinear shape morphing behaviors (between different temporary shapes and the identical permanent shape) can be realized stepwise in a single film via repeated swelling and solvent evaporation with controlled deformations, where the LC alignment and thus different temporary shapes can be introduced, erased, and reprogrammed, respectively, on the fly according to the specific application scenarios.

In surface-aligned LCNs, the degree of alignment within the film thickness (typically ≤100 μm[7] vs. that of our films, 0.4 mm) is highly dependent on the surface chemistry and anchoring strength of LC monomers and chain extenders. Within a printed filament, the degree of LC alignment along the extrusion direction is dependent on the viscosity of the precursor and the printing parameters (e.g., temperature,

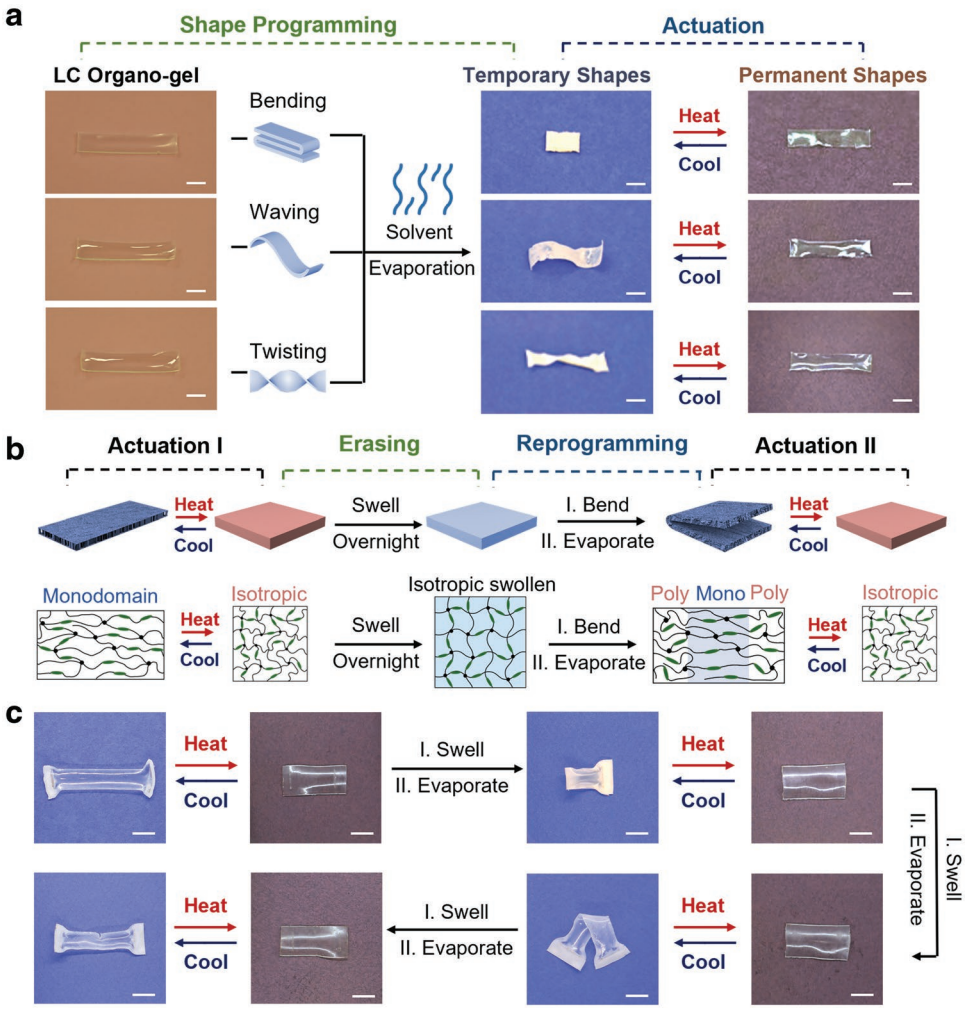

Figure 3. a) Shape programming and actuation via applied spatial deformations during evaporation of toluene. b) Schematic illustrations of the erasing and reprogramming of the LCN for reversible actuation. c) Visual demonstration of the multistage erasing and reprogramming processes for reversible actuation. The sample was reswelled in toluene overnight, followed by solvent evaporation under different modes of deformation. For all samples, toluene is evaporated at 60 °C overnight. Scale bars: 1 cm.

pressure, and speed), all of which need to be controlled to endow the printing and crosslinking synergistically without chain relaxation, which could switch monodomain alignment to polydomain alignment. In our approach, since the network synthesis and mesogen alignment are decoupled, we can create more complex structures, whether permanent or temporary shapes, by post-fabrication programming.

Much like the shape memory polymers (SMPs), the organogel can memorize the deformed shapes after solvent drying. Accordingly, we attempt to transform a 2D LCN sheet into a 3D structure using the origami/kirigami folding strategies,[12] which has so far only been demonstrated in the LCEs with dynamic covalent bonds. Nevertheless, plastic flow could disrupt the LC ordering at the folding lines; the folded structure will be permanently changed once bond exchange occurs.[5] Here, an origami crane (**Figure 4**a) and kirigami pyramid (Figure 4b) can be readily fabricated from a 2D sheet of the organogel via folding, followed by stretching during solvent evaporation, respectively. Upon heating above T_{NI}, the folded shapes can be transformed back to the 2D sheet (Videos S4 and S5, Supporting Information). Although the films are not completely flattened due to the residual stress, which could be minimized by the drying speed, the demonstrated origami/kirigami programming can be applied to many types of LCNs without the specific requirement of surface anchoring strength or low viscosity of the precursors. Besides, the network integrity at the folding lines is not altered, allowing for repeated reprogramming.

3D printing of LCNs offers a powerful tool for 4D programming of shapes with complex geometries. The resolution of the DIW filament is in the range of 150–600 µm. However, LC alignment is degraded when the filament thickness is greater than 100 µm,[6a,b,c] and postprinting UV-curing of the structure is needed to fix the shear-induced alignment. DLP could offer a higher resolution of printed filament (e.g., ≈90 µm[13]). However, because it relies on localized photocrosslinking, not shear-thinning, it is challenging to align LCs within the light focal point without the macroscopic flow of LC monomers or

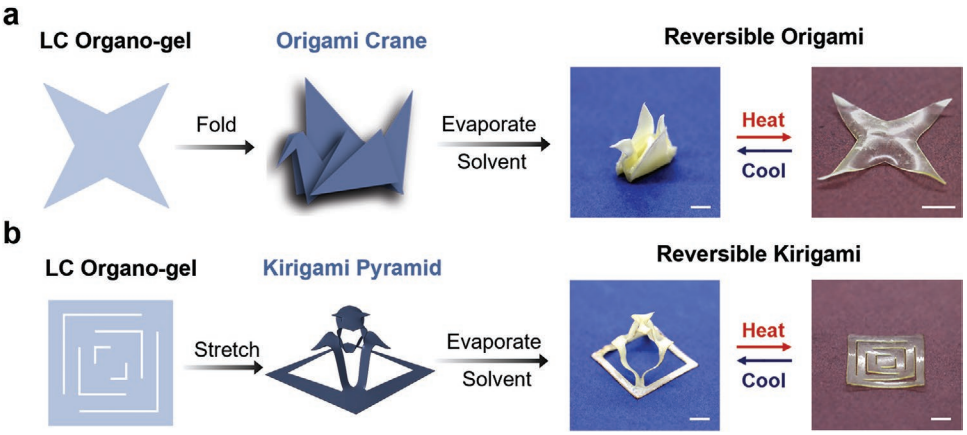

Figure 4. a) Origami crane. b) Kirigami pyramid. Scale bars: 1 cm.

oligomers from the surrounding regions.[13,14] Recently, alignment in DLP printed filaments is demonstrated by shearing the resin tray during printing.[15] Nonetheless, the printed structures are not reprogrammable, and it remains challenging to build complex 3D structures layer-by-layer by this stacked shearing method. In contrast, our approach offers new opportunities to 3D print LCN organogels via DLP first, followed by deformed evaporation to program the shapes as seen in **Figure 5**a. It is noted that RM82-1,3-PDT (the LC oligomer) is replaced with 2,2′-(ethylene-dioxyl) ethanethiol (EDDT; see Figure 5a), a commercial chain extender but less smelly and more user friendly than 1,3-PDT, which is important in an open environment where 3D printer is typically setup. Thus, EDDT is commonly used in 3D printing of LCEs.[6b,11b,13] Moreover, a high solvent mass ratio (67 wt%) can be employed to obtain the proper viscosity (10.10 mPa s; see the Experimental Section), which is critical to the success of DLP printing. A print resolution of 129 µm (Figure S15, Supporting Information) and an actuation strain of 75% (Figure S16, Supporting Information; evaporated with uniaxially stretching) are achieved via our approach. We note that this actuation strain is much larger than those obtained from DIW printed LCEs (typically 30–50%),[6a,b,c] since postprinting stretching is applied here. Meanwhile, the direction of LC mesogens is determined by the poststretching rather than the printing pathway, as confirmed by POM images (Figure S17, Supporting Information), offering unprecedented freedom to print different 3D structures from LCNs via photopolymerization.

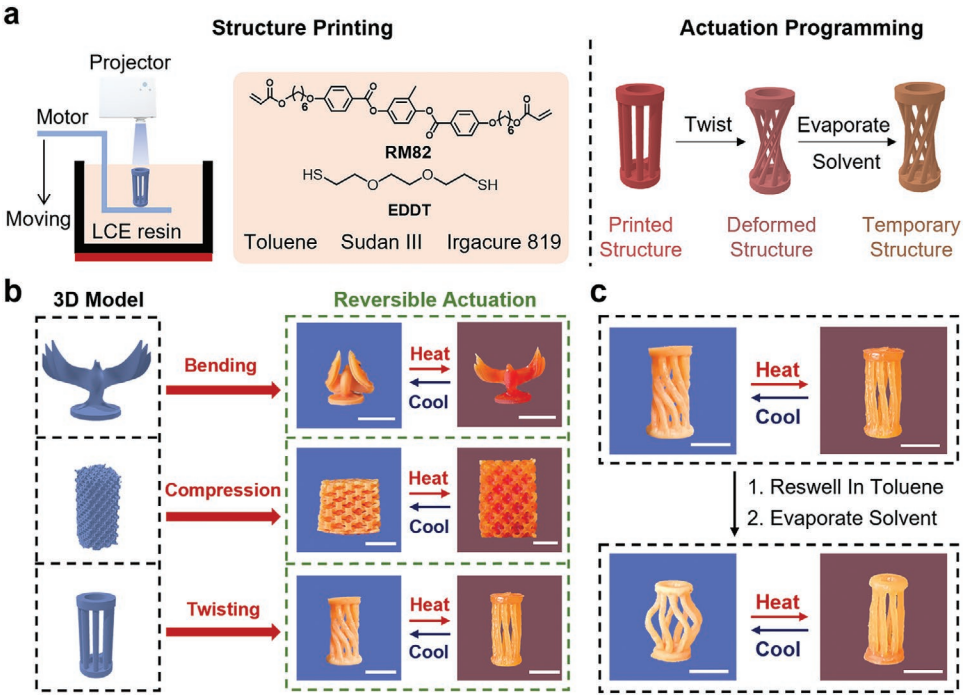

Figure 5. a) The DLP-based 3D printing setup, ink formulation, and programming illustration. b) Three different 3D printed LCN objects and corresponding reversible actuation. For all samples, toluene is evaporated at 60 °C overnight. c) Actuation reprogramming of the pillar structure (from twisting to compression). Scale bars: 1 cm.

The results prompt us to further exploit the potentials of entropic programming of 4D LCNs printed by DLP technique. As seen in Figure 5b a solid crane, a hollow lattice, and a hollow pillar are printed, manifesting the flexibility of our approach in printing and programming both solid and hollow 3D structures. The actuation of the three structures is subsequently programmed globally and locally. In detail, the lattice structure is globally compressed while the wings of the crane and the center of the pillar are locally bent and twisted during the solvent evaporation, respectively. Therefore, the lattice structure performs a homogenous reversible expansion while the wings of the bird and the center of the pillar undergo reversible opening up and un-twisting upon heating (Videos S6–S8, Supporting Information). Since mesogens within the entire 3D printed structures are programmable, globally or locally, the complexity (from one 4D shape to another 4D shape) can be further enhanced via spatial programming. It is noted the postprogramming demonstrated here is different from the preprogramming of DIW printed 3D structures by mechanical stretching of partially cured LCNs.[11] DLP together with entropic programming offer several advantages compared with other 3D printing techniques (Table S2, Supporting Information): 1) higher resolutions and smoother features could be achieved; 2) shear-thinning of LCN precursors is not necessary, thus, easing the printing parameters; 3) solvent swelling and evaporation allows for reprogramming of bulk materials in 3D with hundreds of micron thickness and beyond. As shown in Figure 5c, the reversible twisting/untwisting in the pillar structures can be reprogrammed into a reversible compression/expansion actuation via swelling the sample in toluene for 48 h, followed by evaporation with compression (Videos S9 and S10, Supporting Information).

3. Conclusion

In summary, we demonstrate entropic programming of a solvent-infused LCN organogel by decoupling the network formation and LC mesogenic ordering. Thus, the morphed shapes can be postprogrammed, erased, and reprogrammed at will by controlling the solvent evaporation in an isotropic organogel under stress. Since the LCN structures are not altered during (re)programming, by virtual an infinite number of temporary shapes can be achieved from the same permanent shape with much larger strains than that of prealigned neat LCNs. We further demonstrate the compatibility of our approach with origami/kirigami strategies and DLP printing to create complex temporary and permanent shapes in 4D, respectively. By relaxing the requirements on rheological and mechanical properties on LCNs and the precursors, our approach can be readily adopted by a wide variety of LCN chemistries to achieve good alignment, large actuation strains in a thick film. It could offer new opportunities to pattern and program different types of LCNs separately in the same film, e.g., using orthogonal solvents.[16] It will also shed light to create uniform LCNs over a large area with higher ordered LC phases such as cholesteric and discotic phases and composites with inorganic additives, which are of great interest for dynamic switching of the optical and electronic properties, but have been challenging to fabricate via conventional capillary infiltration due to their high viscosity.[1d,8,17]

4. Experimental Section

Materials: RM82 and 1,4-bis-[4-(3-acryloyloxypropyloxy) benzoyloxy]-2-methylbenzene (RM257) were purchased from Wilshire Technologies. 1,3-PDT was purchased from Sigma-Aldrich, and RM82-1,3 PDT was synthesized following the literature.[7] 2,2-dimethoxy-2-phenyl acetophenone (DMPA), Irgacure 819, 1,8-diazabicyclo [5.4.0] undec-7-ene (DBU), *N*-butylamine, 1,2-ethanedithiol, 1,8-octanedithiol, ethylene glycol bis(3-mercaptopropionate), 1,10-decanedithiol, EDDT, and 1,5-pentanedithiol were purchased from Sigma-Aldrich. Hydrochloric acid (HCl) and magnesium sulfate ($MgSO_4$, anhydrous powder) were purchased from Fisher Scientific. Sudan Red III was purchased from Aladdin. All chemicals were used as received without further purification.

Synthesis of the LC Oligomer (RM82-1,3 PDT)[7]: 10 g RM82 and 3.22 g EDT were dissolved in 200 mL DCM, together with 1.5 wt% DBU as the catalyst. The reaction was kept stirring at room temperature for 20 h. After the reaction, the mixture was washed with diluted 8 wt% HCl aqueous solution twice, followed by washing with DI water once. The DCM was then dried with anhydrous $MgSO_4$ powder for 15 min, followed by filtration. The final LC oligomer was collected as a viscous liquid after evaporating the solvent under vacuum. The molecular weight and distribution were characterized by gel permeation chromatography (EcoSEC HLC-GPC, Tosoh Bioscience LLC).

Synthesis of the Entropically Programmable Liquid Crystal Network (LCN): To investigate the relationship between the actuation strain and the type and mass ratio percentage of the solvent, three different solvents, including DCM, toluene, and DMF were used. RM 82 and RM82-1,3 PDT were mixed at a 1:1 molar ratio in a glass vial, together with 2 wt% DMPA as the photoinitiator, and a desired solvent at a target mass ratio percentage (11, 20, 34, 43, and 50 wt%). The mixture was then stirred at 60 °C to form a transparent solution. After removing the bubble, the precursor was poured into a glass cell sandwiched with a PDMS space (0.4 mm), followed by a UV exposure (Newport model 97436-1000-1, Hg source) at 25 mW cm^{-2} for different durations to completely cure the LC network. After separating the glass cell, an LC organogel was obtained.

Entropically Programming of the LC Organogel: The entropic programming includes two steps: directed solvent evaporation (to direct actuation) and solvent reswelling and free-evaporation (to erase the programmed history). To direct actuation, a rectangular shaped LC organogel film (50 mm × 12.5 mm × 0.4 mm) was uniaxially stretched under a constant force, provided by hanging a weight of mass up to 40 g on one end. The stretched film was then placed into an oven at 25, 60, 80, 120, and 180 °C, respectively, to evaporate the solvent overnight and lock the deformed state. The programming of nonlinear actuation in a planar sheet and 3D printed objects following the same procedure except that the temperature was fixed at 60 °C and the external deformation was maintained by a rigid frame. To erase the programmed director field in the film, the sample was swollen in toluene at room temperature for different durations (0, 0.1, 0.5, 1, 2, and 24 h), followed by free evaporation at 60 °C.

Characterization: The nematic-to-isotropic transition temperature (T_{NI}) of the LC networks was measured by the DSC (TA Q2000). The temperature was scanned from −50 to 200 °C with a ramping rate of 5 °C min^{-1} under N_2.

Porous Structure Characterization: The porous structure was characterized via mercury injection apparatus (Micromeritics, AutoPore IV9510). The tested samples were made from RM82 and RM82-1,3-PDT with different solvent (DCM, toluene, and DMF) and freely evaporated at 60 °C overnight. The solvent mass ratio percentage was fixed at 35 wt%.

Dynamic Mechanical Analysis (DMA): The actuation stability was investigated by DMA (TA Q800) in a control force mode with 0.01 preload force. The analysis of the reversible actuation strain was conducted

under cooling–heating cycles between 30 and 160 °C in ambient air. The ramping rate of the temperature was 10 °C min^{-1}.

Wide-Angle X-Ray Diffraction (WAXD): The X-ray diffraction patterns were collected on the Xeuss 2.0 Dual Source and Environmental X-ray Scattering system with copper source using an X-ray beam of 1.54 Å wavelength, 50.0 kV, 0.60 mA. The sample chamber was under the vacuum environment at 20 °C. All data were collected at a sample distance of 322 mm and calibrated by silver behenate standard. Each sample in alignment introducing step was conducted under the 1000 s exposure and in alignment erasing was 900 s. The data analysis and transformation were done in the DataSqueeze software.

Optical and Electron Microscopy: POM images of the synthesized LCNs with glass slides and PDMS spacer were taken from Olympus BX61 with crossed polarizers. The POM images of the DLP printed film and mesh were taken from NIKON ECLAIPSE E600POL with crossed polarizers. Cross-sectional SEM images were obtained from FEI Quanta 600 environmental scanning electron microscopy (ESEM) at 15 kV electron beam. All the samples were fractured after dipped into liquid nitrogen.

Thermogravimetric Analysis (TGA): The thermal degradation profiles of the LCN films after solvent evaporation was obtained on the Perkin-Elmer Pyris 1 model. The temperature ramped up from 40 to 600 °C at a rate of 10 °C min^{-1} in nitrogen. Specifically, the sample was held at 150 °C for 1 h to determine the amount of residual solvents within the film.

Digit Light Processing (DLP) of LCN: For DLP printing, the LCN was prepared as follows: RM 82 and EDOT were mixed at a 1.05:1 molar ratio in a glass beaker, together with 67 wt% toluene, 3 wt% Irgacure 819 as the photoinitiator, and 0.05 wt% Sudan III as the light absorber. The mixture was stirred at 60 °C for 30 min to form a transparent solution. The temperature of resin was kept at 40 °C during printing to maintain its stability and homogeneity. The DLP printer was assembled from an electric motor and a commercial projector (DELL 1609WX), following the literature.[14] Digital models were produced using AutoCAD. All the printing models were printed using a slice thickness of 100 µm with an exposure time of 20 s, followed by postcuring in a UV chamber (Uvitron Intelliray 600, 66 mW cm^{-2}, 265–700 nm) for 5 min.

Viscosity Characterization: Viscosity of the LCN ink for DLP printing was characterized by a rotary viscosimeter (Shanghai Hengpeng Instrument and Meter Factory, NDJ-5S) at a fixed rotation speed (60 rpm) and temperature (40 °C). The data were averaged over 4 measurements as 10.10 mPa s.

Supporting Information

Supporting Information is available from the Wiley Online Library or from the author.

Acknowledgements

The support to B.J. provided by China Scholarship Council (CSC) is acknowledged. Partial supports by the National Science Foundation (NSF) through the University of Pennsylvania's Materials Research Science and Engineering Center (MRSEC) (DMR-1720530, S.Y.) and the National Natural Science Foundation of China (51822307, Q.Z.) are acknowledged. The authors acknowledge use of scanning electron microscopy and the Dual Source and Environmental X-ray Scattering (DEXS) facility supported by NSF/MRSEC (DMR-1720530) at the University of Pennsylvania. The purchase of DEXS was made possible by an NSF MRI grant (17-25969), an ARO DURIP grant (W911NF-17-1-0282), and the University of Pennsylvania.

Conflict of Interest

The authors declare no conflict of interest.

Data Availability Statement

The data that support the findings of this study are available in the Supporting Information of this article.

Keywords

alignment programming, directed solvent evaporation, liquid crystalline network, shape morphing

Received: October 1, 2021
Revised: November 13, 2021
Published online: December 13, 2021

[1] a) T. H. Ware, M. E. McConney, J. J. Wie, V. P. Tongdiglia, T. J. White, *Science* **2015**, *347*, 982; b) J. Lv, Y. Liu, J. Wei, E. Chen, L. Qin, Y. Yu, *Nature* **2016**, *537*, 179; c)J. Liu, Y. Gao, H. Wang, R. P. Skutvik, C. O. Osuji, S. Yang, *Adv. Intell. Syst.* **2020**, *2*, 1900163; d) S. U. Kim, Y. J. Lee, J. Liu, D. Kim, H. Wang, S. Yang, *Nat. Mater.* **2021**, https://doi.org/10.1038/s41563-021-01075-3.

[2] a) L. Yu, H. Shahsavan, G. Rivers, C. Zhang, P. Si, B. Zhao, *Adv. Funct. Mater.* **2018**, *28*, 1802809; b) A. Buguin, M.-H. Li, P. Silberzan, B. Ladoux, P. Keller, *J. Am. Chem. Soc.* **2006**, *128*, 1088; c) C. M. Spillmann, J. Naciri, B. Ratna, R. L. Selinger, J. V. Selinger, *J. Phys. Chem. B* **2016**, *120*, 6368; d) Y. Xia, G. Cedillo-Servin, R. D. Kamien, S. Yang, *Adv. Mater.* **2016**, *28*, 9637; e) A. Kotikian, R. L. Truby, J. W. Boley, T. J. White, J. A. Lewis, *Adv. Mater.* **2018**, *30*, 1706164.

[3] Y. Wang, A. Dang, Z. Zhang, R. Yui, Y. Gao, L. Feng, S. Yang, *Adv. Mater.* **2020**, *32*, 2004270.

[4] A. W. Hauser, D. Liu, K. C. Bryson, R. C. Hayward, D. J. Broer, *Macromolecules* **2016**, *49*, 1575.

[5] a) P. Zhang, Y. Yang, Q. Chen, E. M. Terentjev, Y. Wei, Y. Ji, *Nat. Mater.* **2014**, *13*, 36; b) Y. Yang, Z. Pei, Z. Li, Y. Wei, Y. Ji, *J. Am. Chem. Soc.* **2016**, *138*, 2118; c) M. K. McBride, M. Hendrikx, D. Liu, B. T. Worrell, D. J. Broer, C. N. Bowman, *Adv. Mater.* **2017**, *29*, 1606509; d) M. K. McBride, A. M. Martinez, L. Cox, M. Alim, K. Childress, M. Beiswinger, M. Podgorski, B. T. Worrell, J. Killgore, C. N. Bowman, *Sci. Adv.* **2018**, *4*, eaat4634; e) Z. Wang, H. Tian, Q. He, S. Cai, *ACS Appl. Mater. Interfaces* **2017**, *9*, 33119; f) D. W. Hanzon, X. He, H. Yang, Q. Shi, K. Yu, *Soft Matter* **2017**, *13*, 7061.

[6] a) A. Kotikian, R. L. Truby, J. W. Boley, T. J. White, J. A. Lewis, *Adv. Mater.* **2018**, *20*, 1706164; b) M. O. Saed, C. P. Ambulo, H. Kim, R. De, V. Raval, K. Searles, D. A. Siddiqui, J. M. O. Cue, M. C. Stefan, M. R. Shankar, T. H. Ware, *Adv. Funct. Mater.* **2019**, *29*, 1806412; c) Z. Wang, Z. Wang, Y. Zheng, Q. He, Y. Wang, S. Cai, *Sci. Adv.* **2020**, *6*, eabc0034; d) Y. Yao, J. T. Waters, A. V. Shneidman, J. Cui, X. Wang, N. K. Mandsberg, S. Li, A. C. Balazs, J. Aizenberg, *Proc. Natl. Acad. Sci. USA* **2018**, *115*, 12950; e) M. Tabrizi, T. H. Ware, M. R. Shankar, *ACS Appl. Mater. Interfaces* **2019**, *11*, 28236; f) S. Woska, A. Münchinger, D. Beutel, E. Blasco, J. Hessenauer, O. Karayel, P. Rietz, S. Pfleging, R. Oberle, C. Rockstuhl, M. Wegener, H. Kalt, *Opt. Mater. Express* **2020**, *10*, 2928.

[7] Y. Xia, X. Zhang, S. Yang, *Angew. Chem., Int. Ed.* **2018**, *57*, 5665.

[8] J. E. Stumpel, E. R. Gil, A. B. Spoelstra, C. W. M. Bastiaansen, D. J. Broer, A. H. J. Schenning, *Adv. Funct. Mater.* **2015**, *25*, 3314.

[9] D. Chen, X. Xia, T. W. Wong, H. Bai, M. Behl, Q. Zhao, A. Lendlein, T. Xie, *Macromol. Rapid Commun.* **2017**, *38*, 1600746.

[10] Y. Hou, G. Fang, Y. Jiang, H. Song, Y. Zhang, Q. Zhao, *ACS Appl. Mater. Interfaces* **2019**, *11*, 32432.

[11] a) K. Liu, F. Hacker, C. Daraio, *Sci. Rob.* **2021**, *6*, eabf5116; b) D. J. Roach, C. Yuan, X. Kuang, V. C.-F. Li, P. Blake, M. L. Romero, I. Hammel, K. Yu, H. J. Qi, *ACS Appl. Mater. Interfaces* **2019**, *11*, 19514; c) M. Barnes, S. M. Sajadi, S. Parekh, M. M. Rahman, P. M. Ajayan, R. Verduzco, *ACS Appl. Mater. Interfaces* **2020**, *12*, 28692.
[12] S. J. P. Callens, A. A. Zadpoor, *Mater. Today* **2018**, *21*, 241.
[13] N. A. Tragutt, D. Mistry, C. Luo, K. Yu, Q. Ge, C. M. Yakaci, *Adv. Mater.* **2020**, *28*, 200797.
[14] S. Deng, J. Wu, M. D. Dickey, Q. Zhao, T. Xie, *Adv. Mater.* **2019**, *31*, 1903970.
[15] S. Li, H. Bai, Z. Liu, X. Zhang, C. Huang, L. W. Wiesner, M. Silberstein, R. F. Shepherd, *Sci. Adv.* **2021**, *7*, eabg3677.
[16] B. P. G. Taylor, J.-K. Lee, A. A. Zakhidov, M. Chatzichristidi, H. H. Fong, J. A. DeFranco, G. G. Maliaras, C. K. Ober, *Adv. Mater.* **2009**, *21*, 2314.
[17] C. Zou, J. Wang, M. Wang, Y. Wu, K. Gu, Z. Shen, G. Xiong, Y. H, L. Jiang, T. Ikeda, *Small* **2018**, *14*, 1800557.